RSC Advances

This is an *Accepted Manuscript*, which has been through the Royal Society of Chemistry peer review process and has been accepted for publication.

Accepted Manuscripts are published online shortly after acceptance, before technical editing, formatting and proof reading. Using this free service, authors can make their results available to the community, in citable form, before we publish the edited article. This *Accepted Manuscript* will be replaced by the edited, formatted and paginated article as soon as this is available.

You can find more information about *Accepted Manuscripts* in the Information for Authors.

Please note that technical editing may introduce minor changes to the text and/or graphics, which may alter content. The journal's standard Terms & Conditions and the Ethical guidelines still apply. In no event shall the Royal Society of Chemistry be held responsible for any errors or omissions in this *Accepted Manuscript* or any consequences arising from the use of any information it contains.

ROYAL SOCIETY OF CHEMISTRY

www.rsc.org/advances

Please do not adjust margins

Journal Name

ARTICLE

Advanced catalyst design induced enhancement of multi-walled nanotube debundling and electrical conductivity of multi-walled nanotube/silicone composite

Received 00th January 20xx,
Accepted 00th January 20xx

DOI: 10.1039/x0xx00000x

www.rsc.org/

Sang-Eui Lee,[a] Shinje Cho,[b] Hajin Kim,[a] Intaek Han[a] and Yoonchul Sohn*[a]

Multi-walled nanotube (MWNT)/silicone composites were fabricated with two different kinds of MWNT bundles grown by catalysts with different morphology. The order of agglomeration of MWNTs turned out to be closely related with the shape of the catalyst particles. Though same composition of precursors was used, catalyst particles made from gelation of the precursors followed by flame synthesis (FS) consisted of chunk-type particles, while those from spray of the precursor solution followed by thermal decomposition (STD) were fabricated with a shape of thin sheets. After CVD growth, the MWNT bundles were entangled to form large masses for FS-catalyst but they maintained rod-like morphology for STD-catalyst. Individual bundle of the STD-MWNTs also contained smaller population of MWNTs with more room inside, which finally resulted in highly conductive MWNT/silicone composite due to effective dispersion of the MWNTs. In this study, for the first time, direct correlation between morphology of MWNT catalysts and electrical conductivity of MWNT/polymer composite was experimentally demonstrated and acquired high electrical conductivity of 1,407 S/m using mass production compatible three roll milling process.

Introduction

Composite materials with polymer matrix and conducting fillers have long been investigated. The conducting fillers include carbon nanotube, graphene[1-3] and metallic materials[4,5]. Carbon nanotube (CNT) has high electrical conductivity and very low percolation threshold due to its one dimensional rod-type morphology.[6] There are many factors known to affect conductivity and properties of CNT/polymer composites. Types of CNT, order of agglomeration of CNT bundles, catalysts to grow CNT, mixing and dispersion process of CNT in polymer matrix, types of the matrix and so on.[7-27]

Many reports on electrical conductivity of CNT/polymer composite materials, including several review papers[7-9], have been published up to now. They can be categorized into several groups. The network of CNT bundles generally showed high electrical conductivity.[10-14] The CNT bundles, having some air gaps in between them, were not completely embedded in polymer matrix and the surfaces of the CNT bundles were coated with various polymers. Y. Ru et al. reported high conductivity of 1.7×10^6 S/m, almost reaching conductivity of pure CNT, with the composite of de-bundled double-walled CNTs doped with chlorosulfonic acid.[10] Nafion-coated single-walled nanotube (SWNT) network showed conductivity of 3,200 S/m (SWNT 18wt.%).[11] However, polypyrrole coated CNT networks presented relatively low conductivity of 21.5 S/m[13] and in-situ polymerized polypyrrole/CNT composite showed 1,600 S/m[14]. Some researchers used one directionally aligned CNTs. T. Souier et al.[15] acquired 350 S/m by infiltrating epoxy into the bundles of multi-walled nanotubes (MWNTs). H. Peng and X. Sun[16] used dropcasting the polymers onto CNT arrays and the composites based on polystyrene and sulfonated poly(ether ether ketones) matrixes showed conductivity of 1,330 and 6,670 S/m, respectively. Use of doped CNTs could also improve electrical conductivities of CNT/polymer composites. The composite with boron doped MWNTs showed high conductivity of 10,000 S/m, 40 times higher than that with undoped MWNTs.[17] In the same way, doping of $SOCl_2$ into SWNTs raised conductivity of the composite from 1,700 to 10,000 S/m.[18]

In general, the composites with CNTs completely embedded in polymer matrix have presented low values of conductivity than the networks of CNT bundles described previously. For example, the composite with MWNTs embedded in polyaniline matrix presented conductivity of 770 S/m, while the network composed of polyaniline coated MWNTs showed higher conductivity of 2,540 S/m.[19] Therefore, high conductivity is rarely found for normal composite materials where CNTs are completely embedded in polymer matrix. The MWNT/epoxy composite[20], the MWNT/SU8 composite[21] and the graphitized CNT/polyoxymethylene composite[22] showed conductivities less than 10 S/m. The poly(dimethylsiloxane) composite having SWNT scaffolds based nano-foams presented electrical conductivity over 100 S/m.[23] The MWNT/ poly(phenylene sulfide) composite[24]

[a] Materials Research Center, Samsung Advanced Institute of Technology, Samsung Electronics, Suwon 443-803, Republic of Korea.
[b] Hanwha Chemical Co. Ltd., 86 Cheonggyecheon-ro, Jung-gu, Seoul, Republic of Korea.
*yoonchul.son@samsung.com

Electronic Supplementary Information (ESI) available: [ESI contains TGA analysis of the MWNTs, conductivity measurement of MWNT powder, viscosity of the MWNT/silicone composites and detailed observation of individual MWNT with TEM]. See DOI: 10.1039/x0xx00000x

RSC Advances Accepted Manuscript

prepared by compression molding showed conductivity of ~1,000 S/m and the SWNT/poly(paraphenylene vinylene) composite[25] also had ~1,000 S/m at SWNT content of 64 wt.%. For this type of CNT/polymer composites, maximum value (~3,000 S/m) was found for the SWNT/polyaniline composite26 and the MWNT/poly (methylmethacrylate) composite having 40 wt.% of MWNTs[27]. In this study, high conductivity of 1407 S/m was obtained at relatively low MWNT content (21.3 wt.%) with an aid of effective debundling of less agglomerated MWNT bundles induced from advanced catalyst design for MWNT fabrication.

Numerous reports about CNT catalysts revealed that morphology of the catalysts had great effect on lateral size of the CNTs grown from the catalysts.[28-32] In general, diameter of the CNTs increased as particle size of the catalysts increased. Therefore, thickness of thin films of metallic catalysts has been reduced to make particle size of the catalysts smaller. G. Zhong et al.[32] acquired vertically aligned single-walled carbon nanotube forests with an area density of 1.5×10^{13} cm^{-2} by using a nanolaminate Fe-Al_2O_3 catalyst consisting of three layers of Al_2O_3, Fe, and Al_2O_3, where the lower Al_2O_3 layer is densified by an oxygen plasma treatment to allow a thinner catalyst layer to be used. However, it has not been reported how fabrication methods of CNT catalysts affect morphology of the catalysts and order of agglomeration of the CNTs grown from the catalysts. In this study, we traced every step to fabricate MWNT/silicone composite: synthesis of the catalysts, CVD growth of the MWNTs, debundling and dispersion of the MWNTs during the process to make the composites. From the experimental results, for the first time, we demonstrate direct correlation between morphology of the catalysts and physical property (electrical conductivity) of CNT/polymer composites. We acquired low density MWNT bundles from thin sheet-like catalysts and MWNT/silicone composite having conductivity of 1407 S/m by optimizing dispersion of the MWNT bundles using mass production compatible three roll milling process.

Experimental

Synthesis of metal catalysts and MWNTs

The catalysts used for MWNT growth consisted of iron, cobalt and aluminium oxide. The iron and cobalt were used as catalysts and aluminium oxide was used for supporting the catalysts. Metal–organic precursors of iron nitrate, cobalt nitrate, and aluminum nitrate were dissolved in water, and then the prepared solution was transformed into catalyst powders by thermal treatment. Two different methods were used to synthesize the catalyst powders : flame synthesis (FS) and spray and thermal decomposition (STD). Flame synthesis was conducted with gelation of the precursors followed by combustion at 500℃. Meanwhile, alternative process was conducted by spraying of the precursor solution followed by thermal decomposition (or oxidation) at 700℃ and final calcination.

The MWNTs used in this study was fabricated with typical chemical vapor deposition (CVD) process using the synthesized catalysts and ethylene gas as a carbon source. The CVD was conducted at 650℃ for 1hr. The fabricated MWNTs are denoted as FS-MWNT and STD-MWNT, respectively after synthesizing methods (flame-synthesis and spray & thermal decomposition).

Fabrication of MWNT/silicone composites

Polydimethylsiloxane (PDMS or silicone), Sylgard 184 purchased from DOW Corning, was used as polymer matrix. In order to disperse the synthesized MWNTs into silicone matrix, two-step shearing process was adopted. A planetary mixer (PDM-1kv, Dae Hwa Tech) was utilized for preliminary mixing. Its rotation and revolution speed were 700 and 600 rpm, respectively. And then ceramic three roll mill (TRM) was applied as primary dispersion process (type C-43/4×10, Inoue). The TRM process is defined as the period between the time for injecting MWNT/silicone mixture into the gap between the 1st and the 2nd roller and the time for collecting the product out of the 3rd roller. The number of TRM repetition and the pressure applied between the rollers, two main processing parameters, were controlled to optimize dispersion of the MWNTs in the composites. The MWNT/silicone pastes were sheared by a film applicator with a shear rate of 100/s to form composite films, which were cured at 130℃ for 30 min in an oven. The cured nanocomposites with a thickness of 1 ± 0.05 mm were used to measure electrical conductivity.

Characterization

Morphology and size of the MWNTs and the MWNT/silicone composites were analyzed with scanning electron microscope (SEM). A field emission-SEM from JEOL inc. (JSM-6700F) was used with an acceleration voltage of 10KV, emission current of 10μA and working distance of 8.0mm. Detailed morphology of individual MWNT was observed with transmission electron microscope (TEM). The H-9000NA model from Hitachi inc. was used with an acceleration voltage of 300kV.

Raman spectroscopy was used to investigate the quality of the MWNTs and their orientation in the composites. The laser was excited at 514 nm with a power of 0.4mW. The grating and acquisition time were 2400gr/mm (extended mode) and 120sec, respectively. Polarized Raman analysis was conducted to analyze aligning direction of the MWNTs in the composites. Spectra acquired with the analyzer set at both perpendicular and parallel to the excitation plane were used to calculate the depolarization ratio.

Thermogravimetric analysis (TGA) was used to characterize thermal property of the MWNTs. The MWNTs in alumina pan were scanned from room temperature to 1000℃ with a scan rate of 10℃/min in air (or nitrogen) atmosphere using METTLER TOLEDO TGA/DSC1. Carbon content was obtained from weight difference between maximum point and final saturation point of TGA curve after subtracting weight increase from oxidation of the catalysts. The oxidation peaks were determined from peak temperature of derivative thermogravimetric analysis (DTG) curve.

A powder resistivity measurement system, HPRM-10D from Hantech inc., was used to analyze electrical conductivity of the MWNT powders. The MWNT powders were put in a vessel with 5mm diameter and volume resistivity was detected

RSC Advances Accepted Manuscript

This journal is © The Royal Society of Chemistry 20xx

while pressure applied on the vessel increased up to 100MPa. Minimum value was extracted as volume resistivity of the MWNT powder.

Results and discussion

Properties of metal catalysts and MWNTs

The catalyst powders synthesized from flame synthesis (FS) and spray and thermal decomposition (STD) are presented in Fig 1(a) and 1(b), respectively. Majority of the former consisted of chunk-type particles whose size ranged from several micrometers to several tens of micrometers. On the other hand, majority of the latter was composed of thin sheets whose thickness was less than 100nm. Before thermal treatment, the precursor of the FS catalyst was treated with gelation method while that of the STD catalyst was finely dispersed during spraying process. Difference of synthetic process resulted in specific particle shape constituting the catalyst powders produced.

The MWNTs grown from flame-synthesized catalyst (FS-MWNTs) were agglomerated with chunk-type morphology. The size of the chunks was measured from several tens of micrometers to several hundreds of micrometers. Each chunk was formed by being entangled with many of individual MWNT bundle as shown in Figure 2(a) and inset. On the other hand, The MWNTs from thermal decomposition synthesized catalyst (STD-MWNTs) consisted of numerous rod-type bundles whose lateral diameter ranged from several micrometers to several tens of micrometers as shown in Figure 2(b). On a large scale, the order of agglomeration was much severer for FS-MWNTs. Furthermore, density of the MWNTs in the bundles was also larger for FS-MWNTs than for STD-MWNTs when we compared the insets in Figure 2(c) and 2(d). It means that order of agglomeration of the MWNTs used in this study was much severer for FS-MWNTs not only on a large scale (collection of the bundles) but also on a small scale (individual bundle). It is noted that morphology of the catalysts is directly related with morphology and agglomeration of the MWNT bundles. In the long run, it will be shown that morphology of the catalysts strongly affected finalized physical property of the composite (electrical conductivity) since percolation and conduction in the composite are controlled by debundling of the MWNT agglomerates.

The characteristics of CVD grown MWNTs were analyzed using SEM, TEM, TGA, Raman and resistivity measurement system and summarized in Table 1. The MWNTs synthesized from both catalysts had lateral diameter of 10~20nm. Number of walls was counted as 8~15 for FS-MWNTs and 9~13 for STD-MWNTs. As was described previously, STD-MWNT bundles showed much lower density than FS-MWNT bundles. Measured bulk density of STD-MWNT powder, 0.015 g/cm^3, was about a half of that of FS-MWNT powder (0.034 g/cm^3). Impurities in the MWNTs were mostly derived from metallic catalysts such as Fe, Co and Al. Content of the impurities was about 3% for both FS-MWNT and STD-MWNT. The STD-MWNT was thermally more stable as shown in Figure 2(e). During the heating process, FS-MWNT started to be decomposed earlier and showed lower oxidation peak temperature (606.7℃) than that of STD-MWNT (657.5℃). Also, see Figure S1 of Electronic Supplementary Information (ESI). Crystallinity of STD-MWNT, analyzed with Raman spectroscopy in Figure 2(f), was also superior to that of FS-MWNT in that STD-MWNT revealed higher value of I_G/I_D (1.05) than that of FS-MWNT (0.92). Consistently, electrical conductivity of STD-MWNT powder was also a little higher than that of FS-MWNT powder (Figure S2 of ESI). As a whole, STD-MWNTs turned out to have better physical properties.

Fabrication of MWNT/silicone composite (optimization of MWNT dispersion)

The MWNT/silicone composites were fabricated with two-step shearing process using a planetary mixer and three roll mill (TRM). For the TRM process, repetition number of TRM and the pressure between the rolls were varied to obtain maximum conductivity of the composites by optimizing alignment of the MWNTs in the composites. As an example, electrical conductivities of the composites having 9.1 wt.% of MWNTs are presented in Figure 3(a) as functions of the number of the milling process and the applied pressure. At the applied pressure of 1.0 MPa, electrical conductivity increased as the number of TRM increased and reached the maximum value after 6 times of repetition. It was saturated with further TRM process. At applied pressure of 2.0 MPa, the same trend was observed until 6 times of TRM repetition but electrical conductivity decreased as the number of TRM increased further. It was found that over-pressure applied on the composite induced damages or breakages on the MWNTs after the optimization of dispersion, which resulted in degradation of electrical conductivity.

With regard to the types of MWNTs used in this study, the composite having STD-MWNTs showed higher electrical conductivity than the composite with FS-MWNTs. After 6 times of TRM process, the fractured surfaces of the composites are presented in Figure 3(b) and 3(c). The surface roughness of the former was apparently larger than that of the latter, as also indicated with the schematics (inset). It may be attributed to order of mechanical networking induced from different MWNT length, which needs further investigation for confirmation. For detailed investigation of the MWNTs in the composite after TRM process, the MWNTs were closely observed after removal of the silicone matrix using a chemical etching process, as shown in Figure 3(d) and 3(e). The etching process was made by submerging a part of the samples in trifluoroacetic acid bath, and then doing a sequence of washing, filtering, and drying. It can be clearly observed that STD-MWNTs are relatively longer than FS-MWNTs after the same number of TRM process, indicating that STD-MWNTs can have better endurance against the harsh dispersion condition of shearing. It may be attributed to the better intrinsic properties, that is, higher powder conductivity, higher straightness and lower I_G/I_D, all of which reflect STD-MWNTs possess a superior crystallinity over FS-MWNTs. High electrical conductivity of the composite

RSC Advances Accepted Manuscript

with STD-MWNTs in Fig. 3(a) can be attributed to better dispersion of longer CNTs.[33] For reference, measured viscosities of both composites were similar for the same MWNT content (Figure S3 of ESI), which confirmed that viscosity of the composites little affect the comparison of the conductivity of the composites with the different types of MWNTs.

Van der Waals force between carbon nanotubes has been studied by many researchers.[34-43] The empirical approach based on the pairwise summation of interatomic Lennard-Jones (LJ) potentials adapted for graphitic structures has been widely applied to explain Van der Waals force between CNTs. In this study, we applied the adapted LJ potentials and the method of the smeared-out approximation suggested by L.A. Girifalco[40,43] to evaluate the potential between two crossed MWNTs. The potentials for the VDW interaction are based on empirical functions whose parameters are obtained from empirical fits to properties of the relevant CNT systems. In the case of MWNT interaction, it is assumed that each pair of layers interacts as SWNTs and use summation over all pairs. In this calculation, we assumed that each MWNT consisted exactly of 11 walls since the MWNTs in this study had 8~15 walls and 11 walls may be chosen as an average value. It was well known that only several outer shells of multi-walled nanotube play an essential role in the VDW interaction. Detailed morphologies of individual MWNT observed with TEM are provided in Figure S4 of ESI.

According to the method of uniform curve[37,39], an approximation for the VDW potential can be expressed by multiplying minimum potential energy (left-hand side of equation 1) with uniform curve (right-hand side). For multi-walled nanotubes with 11 shells,

$$\varphi(d,t_1,t_2,\gamma) \approx \left[\frac{\nu^2}{sin\gamma}\left(C_1\sqrt{t_1t_2}+C_2\frac{t_1+t_2}{\sqrt{t_1t_2}}\right)\right]\cdot\left[b\left(\frac{1}{\left(\frac{d}{d_0}\right)^9}-\frac{b+1}{b}\frac{1}{\left(\frac{d}{d_0}\right)^{\frac{9b}{b+1}}}\right)\right] \quad (1)$$

where d and γ represent the distance between two MWNTs and the angle between two crossed MWNTs, respectively and C_1= -2.161 eV•Å^3, C_2= 1.036 eV•Å^4, d_0=2.87Å, b=0.3. And t_1 and t_2 represent the radii of two crossed MWNTs. Van der Waals force can be derived by differentiating equation (1) with respect to the distance between two crossed MWNTs.

$$F(d,t_1,t_2,\gamma) \approx \left[\frac{\nu^2}{sin\gamma}\left(C_1\sqrt{t_1t_2}+C_2\frac{t_1+t_2}{\sqrt{t_1t_2}}\right)\right]\cdot\left[b\left(\frac{9d_0{}^9}{d^{10}}-\frac{9d_0{}^{\frac{9b}{b+1}}}{d^{\left(\frac{9b}{b+1}+1\right)}}\right)\right] \quad (2)$$

The minimum potential energy (absolute value) increases as the radius of MWNT increases. It is 33.1eV for t_1=t_2=100Å and the value increases up to 49.7eV for t_1=t_2=150Å as shown in Figure 4(a). Meanwhile, the potential energy decreases with increasing angle between two crossed MWNTs. It reaches its minimum value at γ=90° and rises again as shown in Figure 4(b). For the MWNTs with t_1=t_2=120Å, it decreases from 116.2eV for γ=20° to 39.7eV for γ=90°. The values of Van der Waals force are also presented in Figure 4(c) for the case of t_1=t_2=100Å, 120Å and 150Å. They also increase as the radius of MWNT increases and decrease as the crossed angle between two MWNTs increases up to 90°. They increase as the distance between two MWNTs increases and reach zero at d=~2.9Å, finally reaching their maximum values at d=~3.4Å. Two MWNTs within equilibrium distance (~2.9Å) would have repulsive force between them while the MWNTs out of equilibrium distance would have attractive force. For crossed angle of γ=20°, the maximum force increases from 43.3nN for t_1=t_2=100Å to 54.1nN for t_1=t_2=150Å. Therefore, a force larger than 54.1nN should be applied to separate two MWNTs within the distance of 3.4Å. Girifalco et al.[43] explained that all the potentials between two arbitrary CNTs fall on the universal curve when the energy is expressed in units of potential well depth and the equilibrium Van der Waals gap, later verified with C. H. Sun et al. and A. I. Zhbanov et al.[37,39]. Since Van der Waals gap (d) increases with increasing number of walls in CNTs, potential well depth and required minimum force for CNT separation would also increase as number of walls in CNTs increases.

As presented in Figure 2, FS-MWNT bundles showed higher population of MWNTs with larger density than that of STD-MWNTs. It means that more MWNTs in FS-MWNT/silicone composite have to jump the activation barrier to be separated from other CNTs and well dispersed in the composite. Therefore, with same energy applied, the STD-MWNTs would be de-bundled and dispersed more easily than FS-MWNTs in the composite, which resulted in higher electrical conductivity of STD-MWNT/silicone composite. In addition, the rate of MWNT dispersion was also faster for STD-MWNT/silicone composite at early stage of TRM process. Electrical conductivity of STD-MWNT/silicone composite increased about twice than that of FS-MWNT/silicone composite as the TRM process was repeated from one to two times as shown in Figure 3(a).

Electrical conductivity of MWNT/silicone composites

Measured electrical conductivities of MWNT/silicone composites, fabricated with the two-step shearing process using planetary mixer and TRM, are presented as a function of MWNT content in the composites in Figure 5(a) and 5(b). The conductivities were measured after 6 times of repetition of TRM process to reveal maximum conductivity of each composite. For the same MWNT content, electrical conductivity of STD-MWNT/silicone composite was always higher than that of FS-MWNT/silicone composite. For experimentally measured conductivity (in S/m) in a direction parallel to and transverse to MWNT alignment,

$$\sigma = \sigma_0(\Phi - \Phi_c)^t \quad (3)$$

$$\sigma_{STD,||} = 6{,}245(\Phi-0.004)^{0.94} \quad (4)$$

$$\sigma_{STD,\perp} = 6{,}252(\Phi-0.004)^{1.27} \quad (5)$$

$$\sigma_{FS,||} = 4{,}483(\Phi-0.007)^{1.13} \quad (6)$$

RSC Advances Accepted Manuscript

This journal is © The Royal Society of Chemistry 20xx

$$\sigma_{FS,\perp} = 3{,}909(\Phi\text{-}0.007)^{1.28} \quad (7)$$

where σ_0, Φ, Φ_c, and t represent conductivity constant, MWNT content, percolation threshold, and exponent for conductivity behaviour. II and $\perp$ in subscript denote parallel and transverse directions to the shearing direction during the film process, respectively. σ_0 includes information on intrinsic conductivity of fillers, contact resistance between them, and dispersion degree. The higher values of the constant mean that STD-MWNTs in the polymer matrix are superior to FS-MWNTs in the combined effect of the above-mentioned factors, which is consistent with the measured result of the powder electrical conductivity, shown in Table 1. The percolation threshold for STD-MWNT/silicone composite (0.4 wt.%) was lower than that for FS-MWNT/silicone composite (0.7 wt.%). It is attributed to easy debundling and better dispersion of STD-MWNTs in the composite due to low agglomeration of STD-MWNTs as explained previously. It is interesting the percolation threshold is independent on filler alignment direction in both STD-MWNTs and FS-MWNTs, which is the first report for the dependence of the percolation threshold on alignment direction, to our knowledge. The percolation threshold of STD-MWNT/silicone composite is in a similar range with that of SWNT/polyaniline composite (0.3%) having conductivity of ~3,000 S/m.[26] But it is much smaller than that of SWNT/poly(paraphenylene vinylene) composite (1.8%) having conductivity of ~1,000 S/m.[25] The exponents of MWNT/silicone composites in this study (0.94~1.28) are in a smaller level than that of SWNT/polyaniline composite (2.06~2.13) and that of SWNT/ poly(paraphenylene vinylene) composite (2.0). From previous reports[44,45], the exponent is known to have a value of 1.1~1.3 for two dimensional system whereas higher value of 1.6~2.0 was found for three dimensional system. In the viewpoint, both of the composite film in this study may be classified as the two dimensional system. The maximum conductivity of the MWNT/silicone composite was coincided with the conductivity measured in a direction parallel to MWNT alignment through a shear force during film application process. Since electrical current flows through the MWNTs arranged, the conductivity could have the exponent value close to that of two dimensional system.

For the MWNT/silicone system fabricated using TRM process, electrical conductivity in a parallel direction to MWNT alignment,$\sigma_{||}$, was higher than that in a normal direction to MWNT alignment,,$\sigma_{\perp}$, as presented in Figure 5(b). For STD-MWNT/silicone composite, anisotropy ratio of $\sigma_{||}/\sigma_{\perp}$ was 5.9 for MWNT content of 1.0wt.% and 1.8~2.0 for MWNT content over 8.0wt.%. Meanwhile, for FS-MWNT/silicone composite, the anisotropy ratio was 3.5 for MWNT content of 1.0wt.%, 1.8~2.0 for MWNT ~9.0wt.% and finally 1.5~1.7 for MWNT over 17.0wt.%. Therefore, anisotropy of electrical conductivity was higher for STD-MWNT/silicone composite. It is attributed to the fact that the STD-MWNTs can be arranged more easily in horizontal direction of the roller during TRM process since they need less energy for debundling and dispersion in the composite than FS-MWNTs do. For further confirmation of anisotropy of MWNT alignment in the composites, polarized Raman spectroscopy was conducted and the results were presented in Figure 4(c) and 4(d). Intensities of measured Raman peaks showed a clear difference according to the measuring direction. The intensity ratio of Raman peaks parallel to MWNT alignment (I_{XX}) to that normal to MWNT alignment (I_{YY}) was higher for STD-MWNT/silicone composite than for FS-MWNT/silicone composite. The ratio, I_{XX}/I_{YY}, was measured as 2.78 for STD-MWNT/silicone composite while it was determined to be 1.97 for FS-MWNT/silicone composite. The trend was in great consistency with anisotropy of measured electrical conductivities of the MWNT/silicone composites, 2.62 for STD-MWNTs and 2.21 for FS-MWNTs, respectively. The STD-MWNT/silicone composite fabricated with less agglomerated STD-MWNT bundles resulted in low percolation threshold and high electrical conductivity. In the long run, high anisotropy of STD-MWNT alignment was expressed as physical parameters such as Raman intensity and electrical conductivity. This study shows that electrical conductivity of CNT/polymer composite can be controlled by fundamental origin such as morphology of CNT catalysts and order of agglomeration of CNT bundles. The MWNT/silicone composite with high electrical conductivity was achieved by mass production compatible three roll milling process.

Conclusions

The MWNT/silicone composites were fabricated with two different kinds of MWNT sources using two-step shearing process of planetary mixing followed by three roll milling. Density of MWNT bundles could be controlled by synthetic process of metal catalysts. Though same composition of catalyst was used, a catalyst powder made from gelation of the precursors followed by flame synthesis consisted of chunk-type particles, while that originated from spray of precursor solution followed by thermal decomposition was composed of thin sheet-like particles. After CVD growth of MWNTs, the MWNT bundles were entangled to form large masses for the case of FS catalyst, but they stayed with aligned morphology for the case of STD catalyst. In addition, individual bundles of STD-MWNTs also revealed a lower density with more room inside the bundle, which resulted in the composite having higher electrical conductivity due to effective debundling and dispersion of STD-MWNTs.

From the calculation of Van der Waals force between MWNTs having 11 walls, the minimum force for the MWNTs to be separated each other was determined as 54.1nN (for t=150Å). Since highly agglomerated MWNTs have many CNTs to overcome the activation barrier, they would need more energy for debundling and effective dispersion in the composite. As a result, the STD-MWNTs were more easily aligned in horizontal direction to the roller. And the STD-MWNT/silicone composite showed higher electrical conductivity and higher anisotropy of conductivity and Raman intensity measured in parallel and normal direction to MWNT alignment. Through this study, we demonstrated the interplay among the experimental factors such as morphology of the catalysts, order of agglomeration of CNTs grown from the

RSC Advances Accepted Manuscript

catalysts, effectiveness of debundling and dispersion of the CNTs and physical properties of the CNT/polymer composite. The experimental and theoretical findings are important in the viewpoint that this work is the first systematic demonstration revealing the property of CNT/polymer composite are strongly dependent on shapes of catalysts, one of intrinsic characteristics of catalysts.

Acknowledgements

This work was supported by a grant from the Fundamental R&D Program for Technology of World Premier Materials funded by Ministry of Trade, Industry & Energy, Republic of Korea.

Notes and references

1 S. Stankovich, D. A. Dikin, G. H. B. Dommettt, K. M. Kohlhass, E. J. Zimney, E. A. Stach, R. D. Piner, S. T. Nguyen, R. S. Ruoff, *Nature* 2006, **442**, 282.
2 Y. Li, Y. A. Samad, K. Polychronopoulou, S. M. Alhassan, K. Liao, *Sci. Rep.* 2014, **4**, 4652.
3 V. H. Pham, T. T. Dang, S. H. Hur, E. J. Kim, J. S. Chung, *App. Mater. Inter.* 2012, **4**, 2630.
4 Q. Xue, *Euro. Poly. J.* 2004, **40**, 323.
5 Y. J. Li, M. Xu, J. Q. Feng, *App. Phys. Lett.* 2006, **89**, 072902.
6 V. N. Popov, *Mater. Sci. Eng. R.* 2004, **43**, 61.
7 W. Bauhofer, J. Z. Kovacs, *Comp. Sci. Tech.* 2009, **69**, 1486
8 W. Zhang, A. A. Dehghani-Sanij, R. S. Blackburn, *J Mater. Sci.* 2007, **42**, 3408.
9 Z. Spitalsky, D. Tasis, K. Papagelis, C. Galiotis, *Prog. Poly. Sci.* 2010, **35**, 357.
10 E. Muñoz, D. S. Suh, S. Collins, M. Selvidge, A. B. Dalton, B. G. Kim, J. M. Razal, G. Ussery, A. G. Rinzler, M. T. Martinez, R. H. Baughman, *Adv. Mater.* 2005, **17**, 1064.
11 Y. Ryu, L. Yin, C. Yu, *J. Mater. Chem.* 2012, **22**, 6959.
12 B. J. Landi, R. P. Raffaelle, M. J. Heben, J. L. Alleman, W. VanDerveer, T. Gennett, *Nano Lett.* 2002, **2**, 1329.
13 X. Zhang, J. Zhang, R. Wang, T. Zhu, Z. Liu, *Chem. Phys. Chem.* 2004, **5**, 998.
14 J. Fan, M. Wan, D. Zhu, B. Chang, Z. Pan, S. Xie, *J. Appl. Poly. Sci.* 1999, **74**, 2605.
15 T. Souier, S. Santos, A. A. Ghaferi, M. Stefancich, M. Chiesa, *Nanoscale Res. Lett.* 2012, **7**, 630.
16 H. Peng, X. Sun, *Chem. Phys. Lett.* 2009, **471**, 103.
17 C. H. Poa, S. R. P. Silva, P. C. P. Watts, W. K. Hsu, H. W. Kroto, D. R. M. Walton, *Appl. Phys. Lett.* 2002, **80**, 3189.
18 V. Skákalová, U. Dettlaff-Weglikowska, S. Roth, *Synt. Met.* 2005, **152**, 349.
19 E. N. Konyushenko, J. Stejskal, M. Trchová, J. Hradil, J. Kovářová, J. Prokeš, M. Cieslar, J. Y. Hwang, K. H. Chen, I. Sapurina, *Polymer* 2006, **47**, 5715.
20 J. Z. Kovacs, B. S. Velagala, K. Schulte, W. Bauhofer, *Comp. Sci. Tech.* 2007, **67**, 922.
21 C. Grimaldi, M. Mionić, R. Gaal, L. Forró, A. Magrez, *Appl. Phys. Lett.* 2013, **102**, 223114.
22 Y. Zeng, P. Liu, J. Du, L. Zhao, P. M. Ajayan, H. M. Cheng, *Carbon* 2010, **48**, 3551.
23 M. A. Worsley, S. O. Kucheyev, J. D. Kuntz, A. V. Hamza, J. H. Satcher Jr, T. F. Baumann, *J. Mater. Chem.* 2009, **19**, 3370.
24 J. Yang, T. Xu, A. Lu, Q. Zhang, Q. Fu, *J. Appl. Poly. Sci.* 2008, **109**, 720.
25 H. Aarab, M. Baïtoul, J. Wéry, R. Almairac, S. Lefrant, E. Faulques, J. L. Duvail, M. Hamedoun, *Synt. Met.* 2005, **155**, 63.
26 G. B. Blanchet, C. R. Fincher, F. Gao, *Appl. Phys. Lett.* 2003, **82**, 1290.
27 H. M. Kim, K. Kim, C. Y. Lee, J. Joo, S. J. Cho, H. S. Yoon, D. A. Pejaković, J. W. Yoo, A. J. Epstein, *Appl. Phys. Lett.* 2004, **84**, 589.
28 E. F. Kukovitsky, S. G. L'vov, N. A. Sainov, V. A. Shustov, L. A. Chernozatonskii, *Chem. Phys. Lett.* 2002, **355**, 497.
29 A. G. Nasibulin, P.V. Pikhitsa, H. Jiang, E. I. Kauppinen, *Carbon* 2005, **43**, 2251.
30 A. C. Dupuis, *Prog. Mater. Sci.* 2005, **50**, 929.
31 A. R. Harutyunyan, T. Tokune, E. Mora, J. W. Yoo, A. J. Epstein, *J. Appl. Phys.* 2006, **100**, 044321.
32 G. Zhong, J. H. Warner, M. Fouquet, A. W. Robertson, B. Chen, J. Robertson, *ACS Nano* 2012, **6**, 2893.
33 J. Li, P. C. Ma, W. S. Chow, C. K. To, B. Z. Tang, J. K. Kim, *Adv. Func. Mat.* 2007, **17**, 3207.
34 F. London, *Z. Phys.* 1930, **63**, 245.
35 S. M. Gatica, M. M. Calbi, M. W. Cole, D. Velegol, *Phys. Rev. B* 2003, **68**, 205409.
36 S. V. Rotkin, K. Hess, *J. Comput. Electron.* 2002, **1**, 323–326.
37 C. H. Sun, G. Q. Lu, H. M. Cheng, *Phys. Rev. B* 2006, **73**, 195414.
38 E. V. Blagov, G. L. Klimchitskaya, V. M. Mostepanenko, *Phys. Rev. B* 2007, **75**, 235413.
39 A. I. Zhbanov, E. G. Pogorelov, Y. C. Chang, *ACS Nano* 2010, **4(10)**, 5937.
40 L. A. Girifalco, *J. Phys. Chem.* 1992, **96**, 858.
41 T. Schwabe, S. Grimme, *Phys. Chem. Chem. Phys*. 2007, **9**, 3397.
42 I. V. Bondarev, P. Lambin, *Phys. Rev. B* 2005, **72**, 035451.
43 L. A. Girifalco, M. Hodak, R. S. Lee, *Phys. Rev. B* 2000, **62**, 13104.
44 S. Curran, A. B. Dalton, A. P. Davey, B. McCarthy, W. J. Blau, R. C. Barklie, *Phys. Rev. B* 1998, **58**, R7492.
45 S. Kirkpatrick, *Rev. Mod. Phys. B* 1973, **45**, 574.

RSC Advances Accepted Manuscript

 This journal is © The Royal Society of Chemistry 20xx

Journal Name

RSCPublishing

ARTICLE

Table 1 Analyses of the MWNTs used in this study

Characteristics	Sub-category	unit	FS-MWNT	STD-MWNT	Analysis
MWNT morphology (individual CNT)	diameter	nm	10-20	10-20	TEM
	number of walls		8-15	9-13	
MWNT morphology (entangled mass)	diameter (majority)	μm	10-500 (chunk)	2-30 (rod)	SEM
Bulk density		g/cc	0.034	0.015	
Composition	C content	wt.%	96.8±1.3	96.8±1.5	TGA (N_2)
	residue	wt.%	3.2	3.1	TGA (N_2)
	residue constituents	ratio	Fe:Co:Al=2:1:2	Fe:Co:Al=2:1:2	ICP
Thermal stability	oxidation onset	℃	516.6	582.6	TGA (air)
	oxidation peak	℃	606.7	657.5	TGA (air)
Crystalline perfection	I_G/I_D		0.92	1.05	Raman
Powder conductivity	conductivity	S/m	2484±27	2626±34	

RSC Advances Accepted Manuscript

This journal is © The Royal Society of Chemistry 2013

Figure captions

Figure 1. SEM micrographs of the catalysts used for MWNT synthesis : (a) the catalyst acquired from flame synthesis (FS) and (b) the catalyst acquired from spray & thermal decomposition (STD). Scale bars in the pictures and the insets are 1μm and 20μm, respectively.

Figure 2. Morphologies CVD grown MWNTs using (a) FS catalysis and (b) STD catalysis (scale bar : 100μm). Morphologies of individual MWNT bundle grown from (c) FS catalysis and (d) STD catalysis (scale bar : 1μm). (e) TGA analysis curves for FS-MWNT and STD-MWNT (air atmosphere). (f) Raman spectroscopy for FS-MWNT and STD-MWNT.

Figure 3. (a) Measured electrical conductivity of MWNT/silicone composites with regard to repetition number of TRM. SEM micrographs of the fractured surfaces of (b) FS-MWNT/silicone and (c) STD-MWNT/silicone composite. Inset figures are schematics showing the MWNTs with different length and roughness of the fractured surfaces. SEM micrographs of (d) FS-MWNTs and (e) STD-MWNTs after etching silicone matrix. The MWNT content in the composites was 9.1 wt.% and number of TRM repetition was 6 times. The scale bars in the pictures are 1μm.

Figure 4. Calculated potential energy (absolute value) between two crossed MWNTs as a function of (a) the radius of MWNT and (b) the crossed angle. (c) Van der Waals force between two crossed MWNTs, calculated using the method of uniform curve, as a function of the distance between two crossed MWNTs. The MWNTs were assumed to have 11 walls.

Figure 5. (a) Electrical conductivity of MWNT/silicone composites as a function of MWNT content. Percolation threshold and the exponent were extracted from the log scale plot (inset). (b) Measured conductivity in a direction parallel/normal to MWNT alignment in MWNT/silicone composites. Polarized Raman spectroscopy of (c) FS-MWNT/silicone and (d) STD-MWNT/ silicone composites (MWNT 5.66 wt.%). The I_{XX} and I_{YY} peaks were scanned in a direction parallel and normal to MWNT alignment, respectively.

RSC Advances Accepted Manuscript

This journal is © The Royal Society of Chemistry 2012

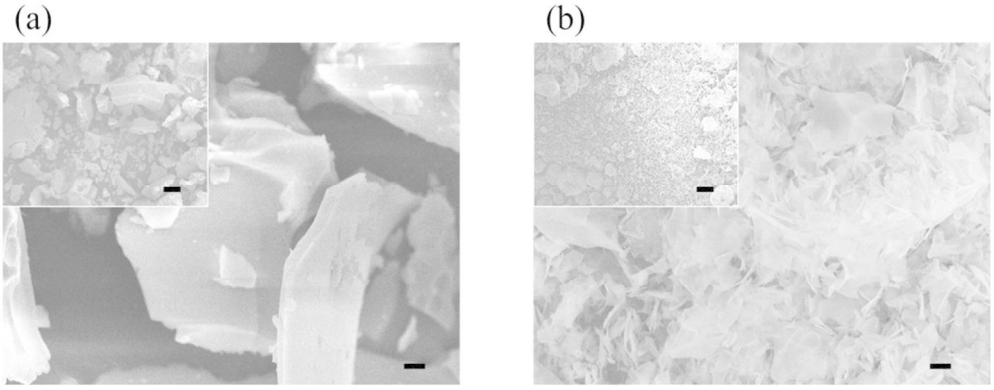

Figure 1. SEM micrographs of the catalysts used for MWNT synthesis : (a) the catalyst acquired from flame synthesis (FS) and (b) the catalyst acquired from spray & thermal decomposition (STD). Scale bars in the pictures and the insets are 1μm and 20μm, respectively.
217x87mm (147 x 147 DPI)

RSC Advances Accepted Manuscript

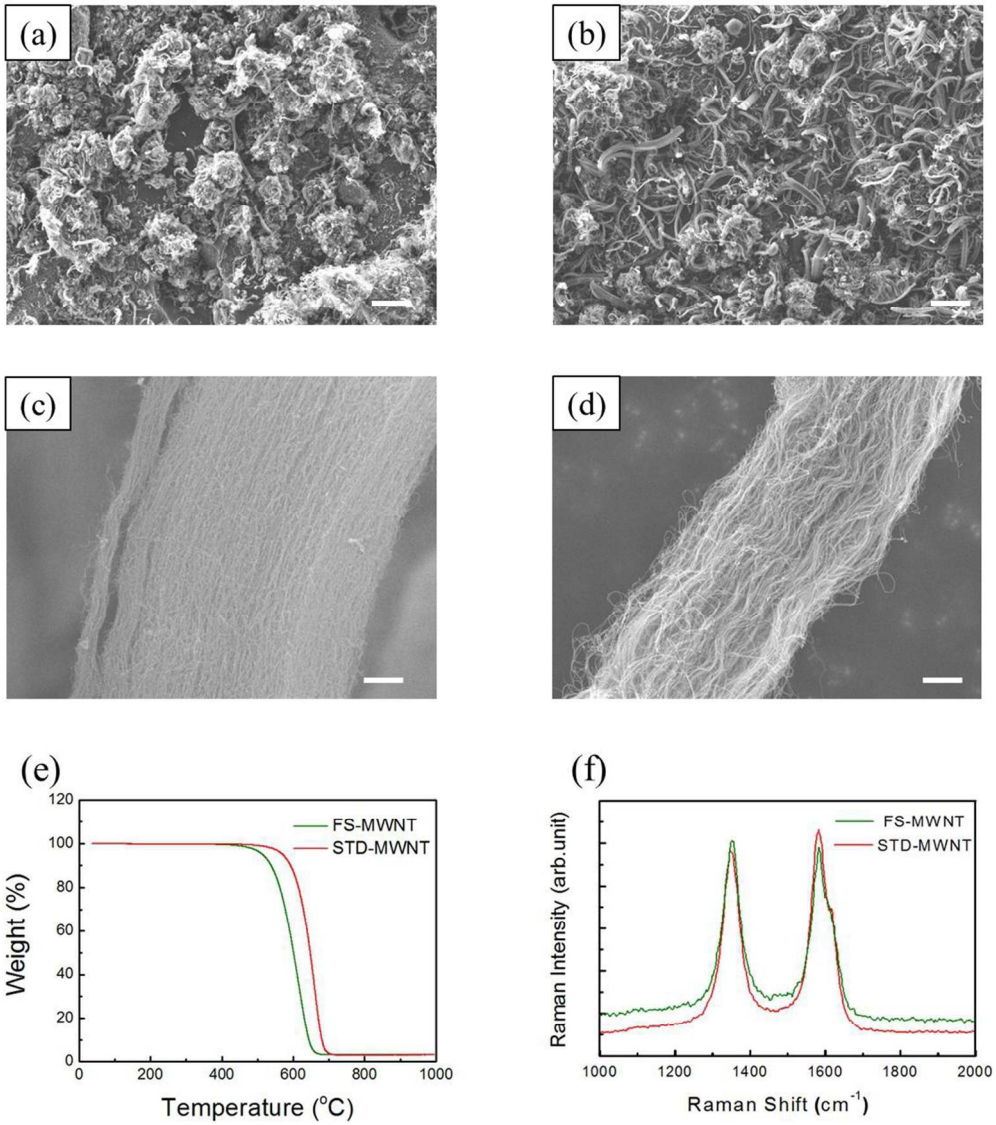

Figure 2. Morphologies CVD grown MWNTs using (a) FS catalysis and (b) STD catalysis (scale bar : 100μm). Morphologies of individual MWNT bundle grown from (c) FS catalysis and (d) STD catalysis (scale bar : 1μm). (e) TGA analysis curves for FS-MWNT and STD-MWNT (air atmosphere). (f) Raman spectroscopy for FS-MWNT and STD-MWNT.
190x215mm (150 x 150 DPI)

RSC Advances Accepted Manuscript

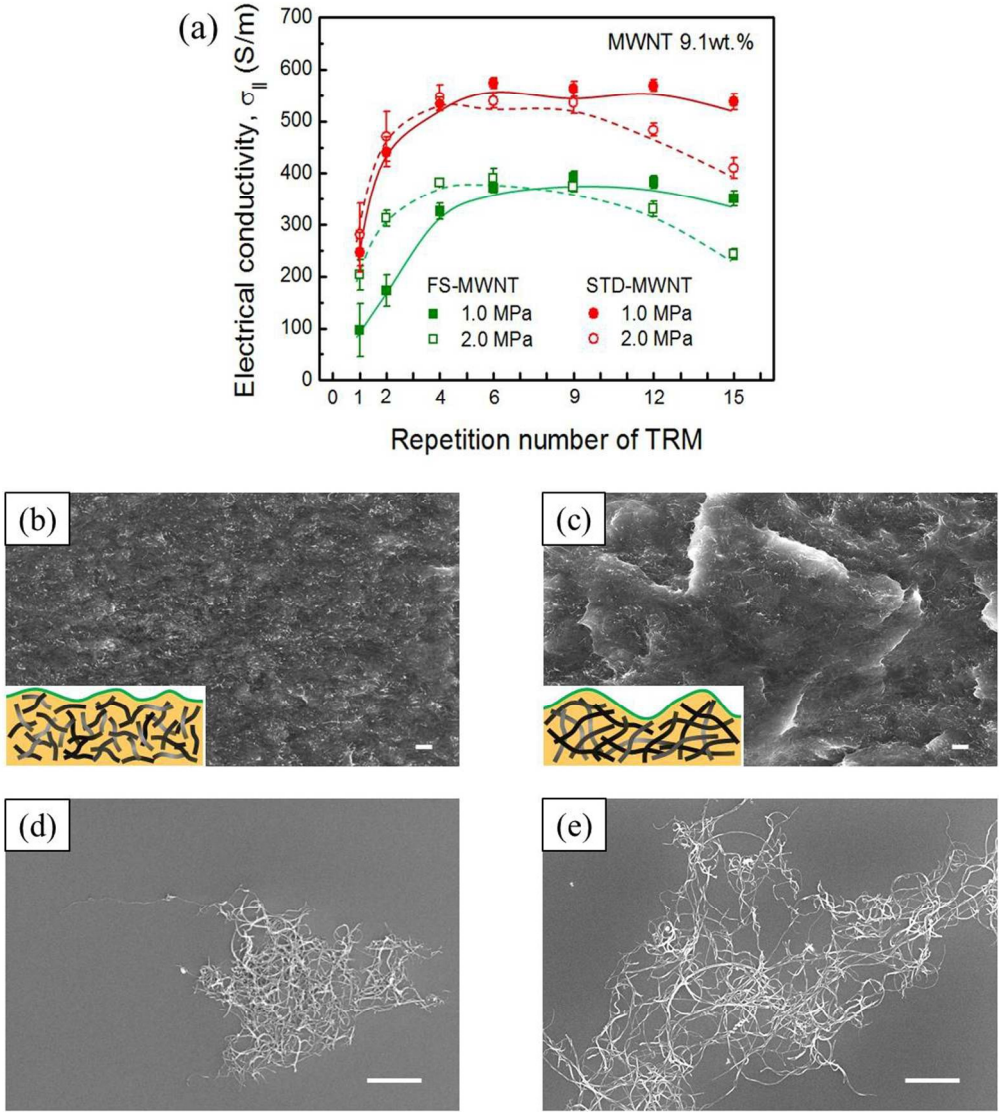

Figure 3. (a) Measured electrical conductivity of MWNT/silicone composites with regard to repetition number of TRM. SEM micrographs of the fractured surfaces of (b) FS-MWNT/silicone and (c) STD-MWNT/silicone composite. Inset figures are schematics showing the MWNTs with different length and roughness of the fractured surfaces. SEM micrographs of (d) FS-MWNTs and (e) STD-MWNTs after etching silicone matrix. The MWNT content in the composites was 9.1 wt.% and number of TRM repetition was 6 times. The scale bars in the pictures are 1μm.
195x218mm (150 x 150 DPI)

RSC Advances Accepted Manuscript

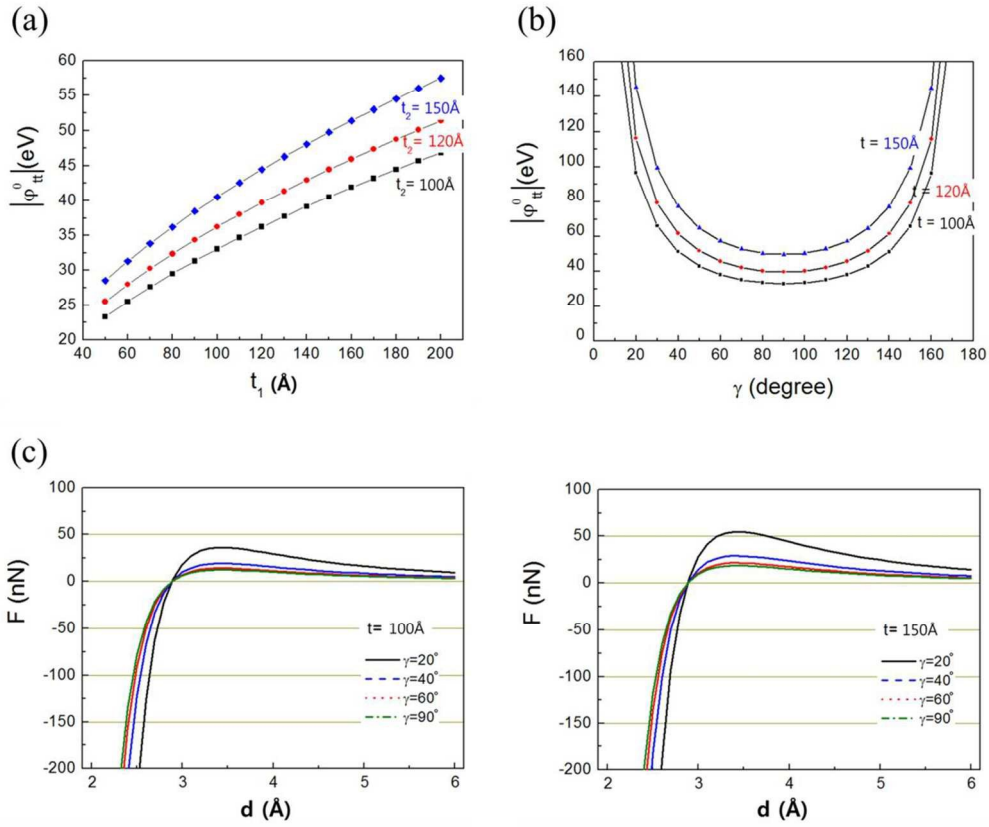

Figure 4. Calculated potential energy (absolute value) between two crossed MWNTs as a function of (a) the radius of MWNT and (b) the crossed angle. (c) Van der Waals force between two crossed MWNTs, calculated using the method of uniform curve, as a function of the distance between two crossed MWNTs. The MWNTs were assumed to have 11 walls.
235x199mm (147 x 147 DPI)

RSC Advances Accepted Manuscript

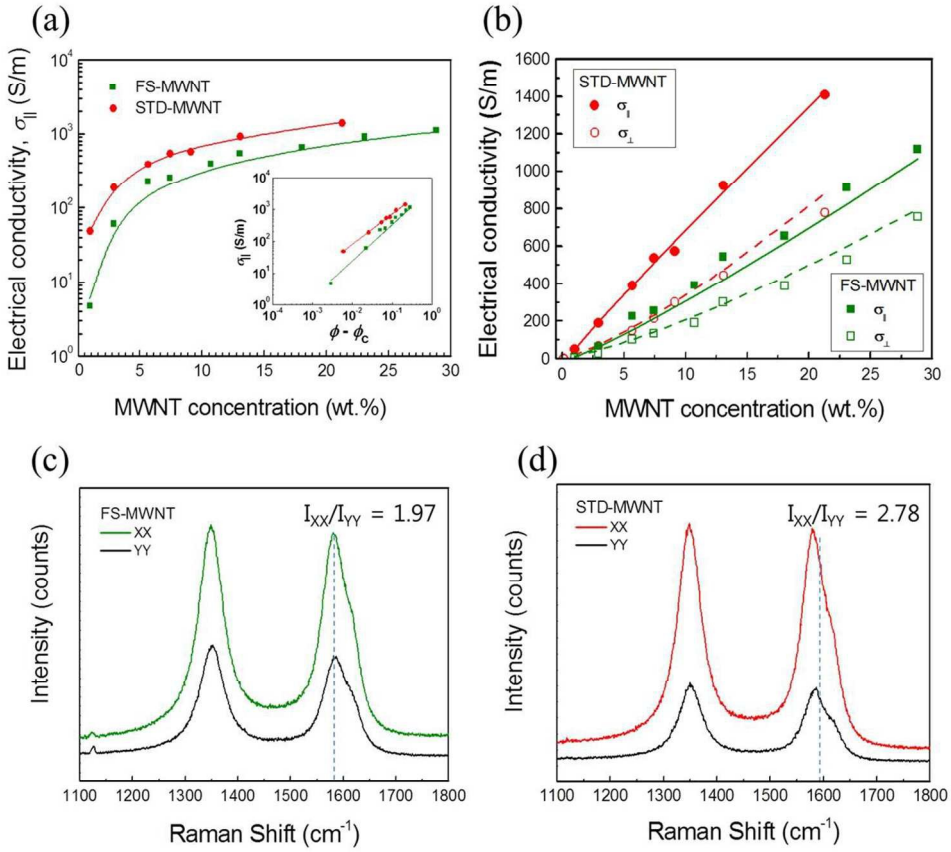

Figure 5. (a) Electrical conductivity of MWNT/silicone composites as a function of MWNT content. Percolation threshold and the exponent were extracted from the log scale plot (inset). (b) Measured conductivity in a direction parallel/normal to MWNT alignment in MWNT/silicone composites. Polarized Raman spectroscopy of (c) FS-MWNT/silicone and (d) STD-MWNT/ silicone composites (MWNT 5.66 wt.%). The IXX and IYY peaks were scanned in a direction parallel and normal to MWNT alignment, respectively.
222x198mm (150 x 150 DPI)

RSC Advances Accepted Manuscript

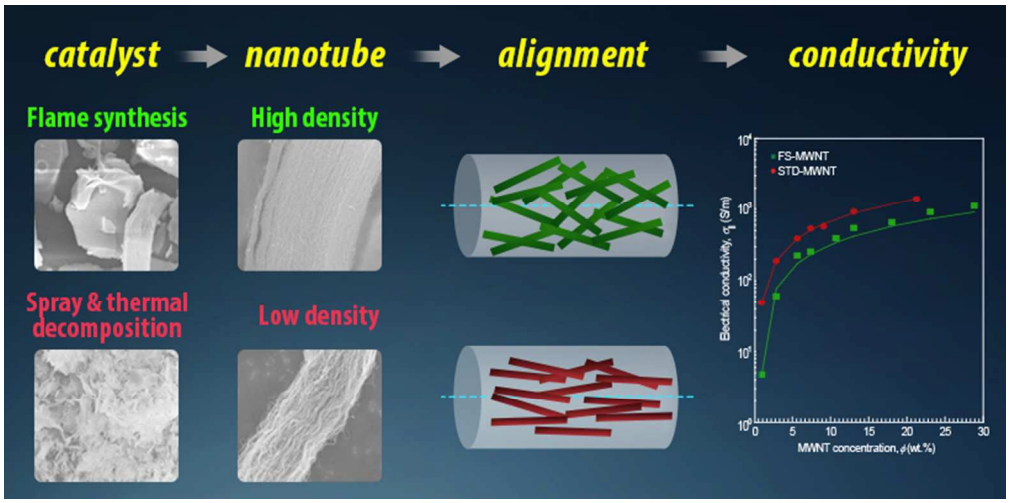

206x101mm (100 x 100 DPI)

RSC Advances Accepted Manuscript